# A Comparison of High Spectral Resolution Infrared Cloud-Top Pressure Altitude Algorithms using S-HIS Measurements

Robert E. Holz, Steve Ackerman, Paolo Antonelli, and Fred Nagle
University of Wisconsin CIMSS
Matthew McGill, Dennis L. Hlavka and William D. Hart
Goddard Space Flight Center

**Will be submitted to:** Journal of Atmospheric and Oceanic Technology

## Abstract

This paper presents a comparison of cloud-top altitude retrieval methods applied to S-HIS (Scanning High Resolution Interferometer Sounder) measurements. Included in this comparison is an improvement to the traditional $CO_2$ Slicing method. The new method, $CO_2$ Sorting, determines optimal channel pairs to apply the $CO_2$ Slicing. Measurements from collocated samples of the Cloud Physics Lidar (CPL) and Modis Airborne Simulator (MAS) instruments assist in the comparison. For optically thick clouds good correlation between the S-HIS and lidar cloud-top retrievals are found. For tenuous ice clouds there can be large differences between lidar (CPL) and S-HIS retrieved cloud-tops. It is found that $CO_2$ Sorting significantly reduces the cloud height biases for the optically thin cloud (total optical depths less then 1.0). For geometrically thick but optically thin cirrus clouds large differences between the S-HIS infrared cloud top retrievals and the CPL detected cloud top where found. For these cases the cloud height retrieved by the S-HIS cloud retrievals correlated closely with the level the CPL integrated cloud optical depth was approximately 1.0.

## Introduction

Cloud altitude is an important parameter in determining the radiative impact of clouds. A standard approach to retrieving cloud-top pressure altitude from infrared satellite observations is the $CO_2$ slicing approach (Chahine 1974: Smith; Wolf et al. 1974: Smith 1978). The method relies on the strong temperature sensitivity of the 15 μm $CO_2$ band and the well-mixed nature of carbon dioxide and was developed to overcome errors in the height retrievals for fields of view that are contaminated with partially cloudy fields or optically thin clouds. The $CO_2$ slicing algorithm has been used successfully to retrieve cloud-top pressure using broadband satellite measurements for over two decades (Menzel; Smith et al. 1983a: Wylie; Menzel 1989). Observations from polar orbiting satellites have yielded a satellite derived global climatology of cloud-top pressure. Today, cloud-top pressure data are derived operationally from the Geostationary Operational Environmental Satellites (GOES) Sounder and Imager instruments (Menzel; Purdom 1994) and used everyday by meteorologists to help interpret current weather conditions. This operational high-cloud satellite product augments cloud height observations from the Automated Surface Observing System (ASOS). The GOES cloud-top retrievals are also used for initializing regional numerical models (Bayler; Aune et al. 2000: Kim; Brown 2002) and in studies of regional distributions of cloud amount and cloud type (Schrieniner; Schmit et al. 2001: Wylie 1994: Wylie; Menzel 1989).

Aircraft based observation of the $CO_2$ 15 μm band at high-spectral resolution have demonstrated improved capability to retrieve cloud-top pressure altitude (Smith; Frey 1990) over narrow band measurements. These aircraft based high-spectral resolution measurements provide the framework to develop new approaches to retrieving cloud-top

pressure that can be applied to new measurements from satellites. This paper presents a new approach to improving retrievals of cloud-top pressure using high spectral resolution infrared measurements. The method is compared with other approaches using passive infrared measurements and also with lidar measurements to assess capabilities with respect to the errors defined by the climate data record accuracy estimates denoted by (Ohring; Wielicki et al. 2002).

This paper will present a new hybrid hyperspectral retrieval algorithm that optimizes the traditional $CO_2$ slicing retrieval by dynamically selecting the optimal $CO_2$ slicing channel pairs. This new algorithm, $CO_2$ sorting, is then compared to fixed channel pair CO2 slicing and Minimum Local Emissivity Variance (MLEV). These three algorithms are applied to hyperspectral aircraft measurements. As part of this investigation the cloud-top retrievals sensitivity to cloud height, partially cloud filled field of views (fov), and cloud optical depth are investigated using collocated cloud lidar and imager measurements.

# Instrumentation

## Scanning High-resolution Interferometer Sounder (S-HIS)

The Scanning High-resolution Interferometer Sounder (SHIS) is an aircraft based scanning Fourier transform interferometer designed to accurately measure atmospheric infrared radiances at high spectral and spatial resolutions (Revercomb; Walden et al. 1998)(Revercomb, H. E. et al., 1998). The S-HIS measures infrared radiances between 400 – 3000 $cm^{-1}$ (3.0 – 25 μm) with a spectral resolution of approximately 0.5 $cm^{-1}$. The radiometric calibration allows for a root-mean squared (RMS) noise errors of less than 0.2 K across the spectral bands except for near the band edges (Revercomb; Walden et al.

1998)(Revercomb, H. E. et al., 1998). The S-HIS has a 100 mrad field of view and is capable of cross scanning. In this paper only nadir fields of view are used in the analysis so that comparisons with nadir viewing lidar can be performed. With a flight altitude of 20 km the nadir S-HIS fields of view have a 2 km diameter surface footprint. The footprint is slightly oval along the flight track due to the 1-second dwell time and 200 m/s along track velocity.

## Cloud Physics Lidar (CPL)

The Cloud Physics Lidar (CPL) is a cloud lidar developed by NASA Goddard that flies on the ER2 high altitude aircraft (McGill; Hlavka et al. 2002). The CPL is an active remote sensing system, capable of high vertical resolution cloud height determinations (30 meters), cloud visible optical depth, and depolarization. Depolarization measurements allows for the discrimination between ice and water. Photons backscattered on the surface of spherical water droplets have very little depolarization in contrast to high depolarization for ice crystals. For CPL measurements clouds with depolarization of greater then 25% are ice while polarizations less than 10% are generally water clouds.

The CPL laser transmits at 355, 532, and 1064 nm and fires 5000 shots/sec. For this paper the 532 nm channel one second averaged data is used for comparison with the passive instruments. The high sample rate of the CPL results in a surface footprint that can be approximated as a continuous line with a diameter of 2 meters. A robust collocation algorithm is used to collocate the CPL measurements with the S-HIS. On average, ten CPL measurements are collocated with each 2-km S-HIS field of view. The collocated CPL measurements of cloud height, depolarization, and optical thickness are used to analyze the sensitivity of S-HIS cloud-top retrievals.

### MODIS Airborne Simulator (MAS)

The MODIS Airborne Simulator (MAS) (King; Menzel et al. 1996) is a scanning spectrometer with a 2.5 mrad field of view. The MAS scene mirror scans at 7.25/sec with a swath width of 42.96° from nadir resulting in a 50-meter nadir surface resolution with a swath width of 37.2 km at the 20 km ER2 flight altitude (King; Menzel et al. 1996). The MAS has 50 spectral channels located within the 0.55 – 14.2 μm spectral region. For this investigation the MAS high spatial resolution is utilized to determine cloud fractional coverage in individual S-HIS fields of view (fov). To identify the MAS pixels within the SHIS footprint, the MAS is collocated with the SHIS using a robust collocation algorithm described in this paper. The results of the collocation are applied to the MAS cloud mask and the cloud fraction of the S-HIS fov is determined (Ackerman; Stabala et al. 1998). In this analysis if the MAS cloud mask determines the pixel to be cloudy or probably cloudy the pixel is designated cloudy. All other classifications are considered clear.

## Analysis Methods

### Collocation of imager and sounder data

The spatial distribution of clouds is highly variable. Quantitative comparisons of multiple instruments with varying fov and scan angles requires that the collocation of the instruments have errors less than the variability of the cloud structure in the fov. For this investigation, a robust collocation algorithm originally developed for satellite collocation is adapted to work with the ER-2 instruments (Nagel 1998). The collocation designates the instrument with the larger fov as the master instrument, in this case the S-HIS. The collocation locates all fov of the secondary instrument or "Slave" instrument (MAS and CPL) that falls within each master fov.

For this application the instruments are located on the same platform (ER-2), simplifying the inverse navigation. The master footprint on the earth's surface is difficult to describe mathematically (Nagel 1998). The collocation uses a simplification described in Figure 1. The surface footprint of the master field of view is approximated as a "radar dish" centered on the surface of the earth. The collocation finds all slave geo-located fov whose angle $\alpha$, measured between the slave geo-location and the center of the geo-located master fov is less than the half angular width of the master instrument.

The geo-location for slave and master instruments is computed using the same geo-location algorithm to reduce errors caused by differences in geo-location algorithms used in the processed data for each instrument. For this reason, the collocation requires the aircraft position, role, heading, altitude, pitch, and instrument scan angle for both instruments. The instrument time is used to narrow the search region for finding collocated slave fov but is not used in the actual collocation. Because the collocation requires only the aircraft navigation information and master instrument fov it is easily adaptable to multiple instruments. This adaptability allows for one algorithm to collocate both MAS and CPL with S-HIS.

While the collocation algorithm is robust, there are approximations and uncertainties. The largest source of errors is caused by the uncertainty of the relative pointing offset from nadir between the master and slave instruments. Each instrument is independently mounted on the ER-2. The angular offset from the aircraft nadir reference for each instrument is not known. It is estimated that errors of 1-2° from actual aircraft nadir may exist. Using an aircraft altitude of 20 km a 2° offset results in a 0.7 km error in the collocation.

To validate the collocated MAS 11μm brightness temperature (BT) was compared to the S-HIS BT. This comparison required convolving the spectral response function of the MAS 11μm channel with the S-HIS measurements to produce S-HIS measurements at the MAS spectral resolution. For each S-HIS fov the collocated MAS pixels are averaged to reduce the MAS spatial resolution to that of the S-HIS. The reduced spectral resolution S-HIS BT with the reduced spatial resolution MAS BT should be very well correlated with an accurate collocation. Any deviations between the instruments BT would result from errors in the collocation of the MAS with S-HIS. This analysis was conducted for both the February 22nd 2003 and December 5th 2003 flights. The February 22-23rd flight had a correlation of 0.97 between 1:07 – 1:32 UTC and for the December 5th flight between 16:30 – 17:00 UTC the correlation between the S-HIS and MAS was 0.99. The slightly lower correlation found for the February 22nd flight most likely results from ER2 navigation data problems during this flight. The high level of correlation between the S-HIS and MAS BT demonstrates the robustness of the collocation.

## $CO_2$ Slicing

The $CO_2$ Slicing algorithm has successfully retrieved cloud-top pressure using satellite measurements for over three decades. The method was developed to overcome errors in the height retrievals of partially cloudy or optically thin fields of view (Smith 1970: Smith; Platt 1978) (Menzel; Smith et al. 1983b). The method relies on the strong temperature sensitivity of the 15 μm $CO_2$ absorption band and the well-mixed nature of carbon dioxide. The $CO_2$ Slicing equation is as follows:

Equation 1

$$\frac{I(v_1)-I_{cl}(v_1)}{I(v_2)-I_{cl}(v_2)}=\frac{\varepsilon_1\int_{ps}^{Pc}\tau(v_1,p)\dfrac{dB\left[v_1,T(p)\right]}{dp}dp}{\varepsilon_2\int_{ps}^{Pc}\tau(v_2,p)\dfrac{dB\left[v_1,T(p)\right]}{dp}dp}$$

Where $I$ is the measured radiance at the spectral region $v_1$, the subscripts reference the two channels selected for the retrieval. $I_{cl}$ is the clear sky radiance, ε is the cloud fractional emissivity, $\tau(v_1,p)$ is the spectral transmittance between the pressure levels $p$ to the instrument, and $B\left[v_1,T(p)\right]$ is the Plank radiance for the selected channel frequency at pressure level $p$. In the current application, both $I(v_{cl})$ and $\tau(v,p)$ are computed using a line-by-line clear-sky radiative transfer model (LBLRTM (Clough; Kneizys et al. 1981)). The temperature and moisture profiles used for the simulations are retrieved using clear sky S-HIS measurements.

The $CO_2$ slicing retrieval assumes the cloud emissivity difference between spectrally close channels is negligible. With this assumption Equation 1 becomes independent of the cloud effective emissivity. The cloud height is then determined by selecting the cloud pressure that minimizes the difference between the right and left side of Equation 1.

In this investigation the fixed channel pair hyperspectral $CO_2$ Slicing algorithm is implemented using the method described (Smith; Frey 1990) using a subset of channels in the $CO_2$ band. Each channel pair is applied to the $CO_2$ Slicing algorithm described in Equation 1. If a unique cloud height is found, the cloud emissivity is computed using Equation 2.

Equation 2

$$N\varepsilon_{c,v} = \frac{I_v - I_{cl,v}}{I_{cld} - I_{cl,v}}$$

If the cloud emissivity is greater than 0.1 and less than 1.0 the channel pair solution is accepted. A cost function is then computed for all valid channel pair solutions as described by

Equation 3

$$\Gamma_v = \sum_{v_{start}}^{v_{end}} \left(I_v - I_{cl,v}\right) - \varepsilon_v \left(I_{cl,v,p} - I_{cl,v}\right)$$

Where $I_v$ is the measured S-HIS radiance in channel v, $I_{cl,v}$ is the calculated clear sky radiance, and $I_{cl,v,p}$ is the calculated opaque cloud radiances at pressure level $p$ determined retrieved using $CO_2$ Slicing. $V_{start}$ and $V_{end}$ represent the channels used as pairs in the retrieval. The cost function finds the channel pair for which the retrieved cloud height and cloud emissivity can best replicate the measured S-HIS channel radiance. The channel pair that minimizes Equation 3 is considered the optimal cloud height.

Appling fixed channel pairs to the $CO_2$ slicing retrieval does not optimize the retrieval sensitivity. The optimal channels to apply to $CO_2$ slicing are dependent on the cloud height. The optimal channels are ones with weighting functions that peak near the cloud attitude. Hyperpsectral measurements have abundant numbers of channels with varying atmospheric opacities and weighting functions. In addition, the decrease in spectral width of the hyperspectral channels results in narrower weighting functions offering the potential for improved vertical resolution (Smith; Frey 1990). However, the large increase in the number of channel pairs introduces the added complexity of selecting optimal pairs (Smith; Frey 1990). If opaque channels are selected whose weighting functions peak well above the cloud height the measured radiance will include

little cloud emission and the $CO_2$ Slicing retrieval will have limited skill. Channels that peak near the cloud-top altitude will maximize the cloud signal, resulting in the largest cloud signal in the left side Equation 1. To maximize the accuracy and reliability of the $CO_2$ slicing retrieval a method to select the optimal channel pairs is required.

## $CO_2$ Sorting

$CO_2$ Sorting is a new algorithm designed to overcome the complexity of choosing the optimal channel pairs needed in the $CO_2$ Slicing. Hyperspectral infrared measurements are capable of resolving spectral features in the 15 μm $CO_2$ band (680 – 770 $cm^{-1}$) (Figure 2). There is a trend to warmer brightness temperatures with increasing wave number due to the decrease in the opacity of the channels. However, the spectral structure of the $CO_2$ band results in significant fluctuation in the opacity of the channels. Assuming an atmosphere that decreases in temperature with height the measured brightness temperatures are proportional to the transparency of the channel. Using this relationship, if the channels are sorted relative to a clear-sky brightness temperature they are also sorted relative to their opacity. This approach is similar to McNally's cloud detection algorithm (McNally; Watts 2003) however in this algorithm the sorting is based on the measured cloud brightness temperature, not the peak of the computed channel weighing functions.

Sorted clear sky brightness temperatures are presented in Figure 2b. The Sorting results in a smoothly increasing function of brightness temperature starting with the coldest most opaque channel to the warmest and most transparent channels in the $CO_2$ band. The Sorting orders the channels by the atmospheric level that the channels weighting function is peaked.

The sorted index of the clear sky sorted spectrum are applied to cloudy fields of view as presented in Figure 3. The most opaque channel whose radiance includes significant cloud emission occurs where the clear and cloudy sorted spectrum deviate. This inflection point is illustrated in Figure 3. The location of the inflection point is a function of the cloud altitude and cloud emissivity. For optically thick and high clouds the channels near the inflection point will have weighting functions that peak above the cloud altitude. Lower or optically thin clouds have inflections points that have weighing functions peaking near the cloud altitude. The weighting functions of the channels selected in Figure 4a are presented in Figure 4b. The cloud height determined using the collocated CPL measurement is included in the figure.

The slope of the sorted cloudy scene is related to the cloud effective emisivity. For optically thick clouds the slope of the cloudy spectrum will converge to the brightness temperature of the cloud. For optically thin clouds there is significant atmospheric emission from below the cloud and the sorted spectrum will not converge to a constant brightness temperature.

It is possible to estimate the cloud height using the brightness temperature of the inflection point. This method will be sensitive to the cloud emissivity and is prone to over estimating the cloud height for optically thick and high clouds. Combined $CO_2$ Sorting and $CO_2$ Slicing overcomes this limitation

## The Hybrid $CO_2$ Slicing/Sorting Cloud Height Algorithm

The $CO_2$ Sorting algorithm offers a tool to overcome the difficulties of selecting optimal channel pairs in $CO_2$ Slicing. The inflection point found by $CO_2$ Sorting represents the first channels with sensitivity to the cloud. Channels after the inflection point on the

sorted spectrum will have cloud sensitivity. The hybrid $CO_2$ Slicing/Sorting retrieval dynamically selects the channels to apply to $CO_2$ Slicing using only channels after the inflection point on the sorted spectrum. To reduce cloud height errors due to uncertainties in the surface temperature, emissivity, and lower tropospheric water vapor and temperature profile $CO_2$ Sorting selects channels located between the inflection point and the first channel on the sorted spectrum determined to have significant surface emission. For a clear sky fov the sorted spectrum will converge to a constant brightness temperature as the channels gaseous optical depth becomes small so that the signal measured in the channel is dominated by surface emission. The $CO_2$ sorting algorithm uses this decrease in slope to determine if the channel has significant surface emission. Only channels on the sorted spectrum between the inflection point and the first channel determined to have significant surface contribution are selected as possible channels. To further optimize the channel selection it was found that channels in the valleys of the $CO_2$ absorption region (650 – 800 $cm^{-1}$) produced the most consistent cloud height results.

For this reason only the channels selected by $CO_2$ Sorting that are located in the valleys in the $CO_2$ absorption region are applied to $CO_2$ Slicing.

## MLEV

Minimum Local Emissivity Variance (MLEV) is a cloud-top retrieval algorithm designed to take advantage of hyperspectral measurements (Huang; Smith et al. 2003). MLEV uses the spectral channels between 750 – 950 $cm^{-1}$ that includes $CO_2$ and water vapor absorption lines(Huang; Smith et al. 2003). The ability of the hyperspectral infrared measurements to resolve the line structure allows for the calculation of cloud Emissivity (Equation 2) across the absorption spectrum. In contrast to the atmosphere, clouds have

very little spectral structure across these wavelengths. The calculation of the cloud emissivity requires that the cloud altitude be known in order to calculate $I_{cld}$ in the denominator of Equation 2. With an incorrect cloud height the spectral structure of the absorption line will not cancel in Equation 2 resulting in large spectral variability in the emissivity calculation. The cloud height that minimizes the spectral variability in Equation 2 yields the best cloud height estimate. The MLEV solving equations are illustrated in Equation 4 and Equation 5. In these equations $I_\nu$ is the measured cloud radiance for channel $\nu$, $I_{cld,\nu}$ is the calculated opaque cloudy radiances, $I_{cl}$ is the calculated clear sky radiance, $N$ is the cloud fraction, and $\varepsilon$ is the cloud emissivity. The cloud fractional emissivity is calculated for the channels between 750 –950 cm $^{-1}$ at each pressure level $P_c$. The pressure level that minimizes the spectral variation in this channel interval is considered the cloud pressure level. The implementation of MLEV requires calculations of the cloudy radiances at each pressure level given in the temperature and moisture profile. For this analysis LBLRTM was used for these calculations using the S-HIS and dropsondes for water vapor and temperature profiles.

Equation 4

$$LEV(P_c) = \sum_{\nu_1}^{\nu_2} (N\varepsilon_{c,\nu} - \overline{N\varepsilon_{c,\nu}})^2$$

where

Equation 5

$$\overline{N\varepsilon_{c,\nu}} = \frac{\sum_{\nu-(\Delta/2)}^{\nu+(\Delta/2)} (N\varepsilon_{c,\nu})}{\Delta\nu}$$

## Cloud Height Retrieval Validation

The hyperspectral cloud-top retrieval algorithms are applied to S-HIS measurements during THORPeX Pacific based in Hawaii (Shapiro; Thorpe 2002) and ACTReX field campaign (Shapiro; Thorpe 2002) based in Bangor Mane. The THORPeX field campaigns are part of the Global Atmospheric Research Program (GARP) goal of improving 1 to 14 day weather forecasts. For both missions the S-HIS flew with the CPL and MAS on the NASA ER2 aircraft. These field campaigns where selected for their diverse clouds and atmospheric environments. In the following analysis the hyperspectral cloud-top retrieval algorithms are applied to selected flight segments. The results are compared to collocated CPL and MAS measurements.

### THORPEX Pacific

#### ER2 Flight Track 01:07 – 02:00 UTC

As part of the THORPeX field program on February 22nd 2003 the ER2 flew over the Pacific Ocean west of Hawaii. During the flight high cirrus clouds with tops at 12 –13 km where detected by the CPL (Figure 5). The CPL cloud extinction profile in Figure 5 shows that the cloud extinction increases towards the lower levels of the cloud. The CPL measured depolarization remains above 25% except near 01:40 UTC where the cloud depolarization is as low as 20%. As previously discussed depolarization greater than 25% signify ice. It would be unusual to have liquid water above 10 km. A possible explanation for the low depolarization is a change in ice habit, perhaps small droxtals as the amount of depolarization is dependent on the ice crystal shape.

Figure 6 presents the S-HIS cloud-top retrievals with the collocated CPL cloud boundaries. The CPL has a maximum optical depth sensitivity of approximately 3.2 (McGill 2004). For this reason, when interpreting the CPL cloud boundaries the actual cloud geometrical thickness may be larger than presented in Figure 6 if the actual cloud optical depth is greater than 3.2. If the CPL does not detect a lower cloud or ground return the CPL retrieved cloud base is not presented. The S-HIS cloud fraction in Figure 6 is retrieved by applying the MAS cloud mask algorithm to the collocated MAS pixels within each S-HIS fov.

The region between 1:15 – 1:30 UTC show the largest variations compared to the CPL cloud height. For this period the cloud optical depth remains small with the collocated CPL optical depth measurements ranging between 0.5 – 2.5. The largest differences were found when the cloud fraction is less than 1.0 at approximately 1:27 UTC. The optically thin cloud presents a challenging environment for the S-HIS cloud-top altitude retrievals. For this period, the $CO_2$ hybrid Slicing/Sorting algorithm results demonstrate the closest agreement to the CPL cloud height. The fixed $CO_2$ Slicing and MLEV retrievals significantly underestimate the cloud-top. The largest differences between the CPL and SHIS cloud heights occur at 1:27 UTC when the S-HIS fov is partially cloud filled as determined by the MAS cloud fraction.

After 1:30 UTC the cloud optical depth remains greater than 3.0 for most of the profile as determined by the CPL. Between 1:30 – 1:35 UTC there is good agreement between the S-HIS and CPL retrieved cloud-top altitude. After 1:35 UTC the S-HIS and CPL cloud-top altitude diverge with the S-HIS retrievals underestimating the cloud-top

altitude. By 1:45 UTC the S-HIS retrieved cloud-top retrievals for the three algorithms differs by as much as 2.5 km compared to the CPL.

The distribution of the differences between the collocated CPL measured cloud-top height compared to the S-HIS cloud-top height retrieval is presented in Figure 7. The differences between the CPL and S-HIS are calculated using the mean cloud top height of the CPL measurements found for each S-HIS fov. A negative difference results if the SHIS retrieval is lower than the CPL retrieved cloud height. Figure 7 confirms that the there is significant variability between the CPL and S-HIS cloud-top altitude retrievals. The fixed channel $CO_2$ slicing and the hybrid $CO_2$ slicing/sorting compare closely with mean differences of -1.40 and -1.34 km while MLEV demonstrates a tendency to overestimate the cloud height with a mean difference of +0.79 km. The width of distributions differed significantly with the hybrid $CO_2$ slicing/sorting having a significantly narrower distribution of +/- 0.65 km compared to fixed channel $CO_2$ slicing and MLEV with standard deviations of +/- 1.36 and 5.67 km..

The differences in the sensitivities between the three algorithms becomes apparent when only S-HIS fovs with collocated CPL cloud optical thickness less then 1.0 are considered as presented in Figure 8. For optically thin clouds the hybrid $CO_2$ slicing retrieval significantly reduces the cloud height biases with a mean of -0.89 km compared to -1.9 and +3.0 for the fixed channel $CO_2$ Slicing and MLEV.

## ATReC Atlantic

The ER2 flew during the ATReC field experiment based in Bangor, Maine, in the fall of 2003 as part of the Global Atmospheric Research Program (GARP). In addition to the MAS, CPL and S-HIS on the ER2 the NOAA G-4 and Citation flew during the

experiment with an extensive array of insitu measurements. This paper will focus on the December 5th 2003 ER2 flight that over flew a variety of cloud types ranging from high cirrus to stratus. Two different ER2 flight tracks are selected for their variety of cloud types.

## ER2 flight track 16:30 – 1700 UTC

The ER2 flight segment between 16:30 – 17:00 is characterized by diverse cloud conditions. The CPL measured cloud-top and depolarization measurements indicate rapidly changing cloud height and phase as presented in Figure 9. The CPL measured cloud depolarization varies between 2.0% and 50% signifying a mixed phase environment.

The S-HIS cloud-top altitude retrievals collocated with the CPL and MAS retrieved cloud properties are presented in Figure 10. The S-HIS cloud top retrievals show good agreement with the CPL cloud top heights during this flight segment. The beginning of the flight segment (16:30 – 16:37) demonstrates the greatest variability between the S-HIS and CPL cloud top retrievals with all three retrievals overestimating the cloud height. Broken and multilevel clouds characterize this time period as determined by the collocated CPL and MAS measurements. Between 16:37 – 16:50 UTC all the S-HIS cloud-top retrievals detect the cloud with good agreement with the CPL.

The peak of the hybrid $CO_2$ Slicing/Sorting difference distribution presented in Figure 11 compares closely with the CPL cloud heights with mean differences less then 1.0 km for all three retrievals. The tendency for the cloud top retrievals to overestimate the cloud height when the S-HIS fov is partially cloud filled is apparent in Figure 11 as the small peak with positive differences (S-HIS retrieved cloud height is above the CPL).

The peak is most pronounced for MLEV but all three algorithms overestimate the cloud height for broken clouds.

### ER2 flight track 18:00 – 18:50 UTC

The beginning of the flight segment (18:05 – 18:30) contains broken mid-level clouds with a thin cirrus layer over low stratus existing between 18:26 – 18:28 UTC. The hybrid $CO_2$ Slicing/Sorting and the fixed channel pair $CO_2$ Slicing retrieval detects the midlevel cloud but has considerable variability compared to the CPL cloud height. MLEV has less variability but consistently over estimates the cloud height as presented in Figure 14.

The flight segment after 18:30 UTC consists of low marine broken cumulous which progressively becomes overcast based on the MAS derived cloud fraction in Figure 13. Between 18:33 – 18:39 UTC the hybrid $CO_2$ Slicing and MLEV do not detect the broken cumulous while the fixed channel $CO_2$ Slicing infrequently detects the cumulus. When the fixed channel $CO_2$ does retrieve the cloud height it overestimates the cloud top.

After approximately 18:40 UTC the broken cumulus becomes overcast based on the MAS cloud fraction. This coincides with both $CO_2$ Slicing algorithms retrieving a cloud height that consistently overestimates the cloud height compared to the CPL.

## Discussion

This paper has presented a comparison of infrared hyperspectral cloud-top altitude retrieval algorithms including $CO_2$ Sorting/Slicing, a new hyperspectral cloud-top retrieval. The following discussion will interpret the results using the collocated MAS and CPL measurements with a focus on the periods when there was disagreement between the S-HIS and CPL cloud-top altitude retrievals.

When combined with $CO_2$ Slicing, the Sorting significantly improves the cloud-top altitude retrieval for optically thin clouds compared to the fixed channel pair $CO_2$ Slicing alone. For optically thin clouds the difference between the measured cloudy radiance $I(v)$ and the clear sky simulated radiance $I_{cl}(v)$ in the $CO_2$ Slicing equation (Equation 1) becomes small with measured minus clear differences less then 2 ($mw\ str^{-1}\ \mu m^{-1}$). For this reason $CO_2$ Slicing becomes very sensitive to the accuracy of the clear sky radiance calculation, which is dependent on the a priori knowledge of the lower atmospheric temperature, water vapor, and surface temperature and emissivity. The hybrid $CO_2$ Slicing retrieval reduces the cloud retrieval biases for thin clouds by selecting channel pairs that maximize the sensitivity to the cloud level but not the surface. Reducing the surface contribution reduces the retrieval sensitivity to errors in the lower atmospheric state. The hybrid $CO_2$ Slicing/Sorting algorithm has the smallest altitude bias based on a comparison with the collocated CPL cloud heights for thin clouds (optical depths less then 1.0) as highlighted in Figure 8. Notice that the hybrid $CO_2$ slicing retrieval eliminates the large 4 – 5 km cloud height differences observed using fixed channel $CO_2$ Slicing and MLEV

Large differences (greater than 3 km) in cloud-top altitude retrievals between the S-HIS and the CPL occurred in Figure 6 between 1:25 – 1:55 UTC. The cloud as detected by the CPL cloud extinction in Figure 5 is geometrically thick but optically tenuous cirrus. This case represents a condition where the different sensitivities between the CPL and S-HIS can result in large differences in the retrieved cloud-top height. The CPL measures the backscattered intensity while the S-HIS measures primarily atmospheric emission. The intensity of the backscatter measured by the CPL is a function of the cloud

backscatter cross-section while the S-HIS cloud signal is a dependent on the cloud optical depth. Cirrus microphysical properties can result in a significant lidar return well above the level at which the integrated cloud optical depth becomes large enough to be detected by the S-HIS retrievals.

To investigate the differences found in Figure 6, collocated CPL extinction profiles are integrated starting from the top of the cloud to produce integrated optical depth contours at each CPL level in the cloud. Using the integrated CPL extinction, the integrated optical depth at the level the S-HIS retrieval detected the cloud is determined as illustrated Figure 15.

The geometric S-HIS – CPL cloud height differences and integrated optical depths using the method described in Figure 15 for the February 22 flight between 1:30 – 1:50 UTC are presented in Figure 16 and Figure 17. The S-HIS –CPL cloud height differences progresses from relatively close agreement at 1:30 UTC to differences larger than 2.5 km at 11:45 UTC. Despite the large geometric differences, the integrated optical depth at the level the S-HIS detected the cloud height remains relatively constant between 0.5 – 1.0. The distribution of integrated optical depths at the level of the S-HIS retrieved cloud height in Figure 17 shows a sharp peaked at optical depth 0.75.

This result illustrates the importance of considering the instrument sensitivities to cloud microphysical characteristics when comparing cloud height results. It raises the question; what is the correct cloud-top height when two independent measurements can accurately measure the cloud height but differ by more than 2.5 km? The answer depends on the on the application. For infrared cloud radiative processes the S-HIS cloud-top retrieved altitude may be a more representative measurement while the lidar

cloud-top is best applied to visible cloud characteristics. When lidar measurements are used to validate infrared cloud-top altitude retrievals this result suggests that the lidar retrieved integrated extinction is a more representative measurement when comparing to infrared cloud-top retrievals.

This result has important implications for satellite cloud height validation. Global lidar measurements of cloud heights are currently available using GLAS (Schutz 1998) data and will soon be available with the launch of CALIPSO (Winker; Wielicki 1999). These measurements allow for global cloud climatology with extremely high vertical resolution and sensitivity to optically thin clouds. In addition, the measurements offer a validation data set to compare to infrared cloud retrievals such as MODIS and AIRS. The results in this investigation suggest that for geometrically thick but optically thin cirrus large differences between the lidar and passive IR remote sensed cloud-top heights should be expected and that these differences may represent differences in the instrument sensitivities, not errors in the retrievals.

Low clouds (below 3.0 km) present a challenging environment for IR cloud retrievals. As previously discussed the largest uncertainties in the temperature and water vapor profiles are in the lower atmosphere. To compound the difficulties for low clouds the difference between the cloud and surface temperatures are small further reducing the cloudy minus clear sky difference in Equation 1. As expected the largest differences between the S-HIS cloud-top retrievals and the CPL where for low clouds.

The ability for the $CO_2$ sorting to detect low clouds depends on the clear sky fov. For this investigation the clearest fov for the flight track was selected by using the fov with the warmest window brightness temperature. A cloud contaminated clear sky fov

will degrade the already weak contrast between low clouds and the sorted clear scene reducing the reliability of the sorting algorithm channel selection. Additionally, the hybrid $CO_2$ Slicing purposefully rejects channels that have significant surface sensitivity. If the cloud is very near the surface the hybrid algorithm will pick channels that peak above the cloud further reducing the sensitivity. Future work will address this issue by using selected channel pairs that are optimized for low clouds when $CO_2$ sorting determines low clouds in the fov. An alternative would be to use a water vapor corrected brightness temperature retrieval.

The fixed channel pair $CO_2$ slicing uses fixed micro-window channels in the $CO_2$ band (740 –800 $cm^{-1}$). The relatively transparent micro windows have weighting functions that peak near the surface. For low clouds these channels should optimize the $CO_2$ slicing retrieval possibly explaining the increased sensitivity for low clouds. The MLEV retrievals lack of sensitivity to low clouds supports the findings of (Huang; Smith et al. 2003).

The ability to detect and retrieve cloud heights is dependent on the accuracy of the clear sky temperature and water vapor profile used to simulate the clear sky radiances used in the retrieval. For this investigation well characterized atmospheric profile information was available using S-HIS temperature and water vapor retrievals and aircraft dropsonds. For satellite retrievals global temperature and water vapor profiles are required. The accuracy of the atmospheric profile measurements will impact the sensitivity and accuracy of the retrievals, especially for optically thin or low clouds. The hybrid $CO_2$ Slicing/Sorting retrieval has the potential to reduce cloud height errors caused by atmospheric profile uncertainties.

## Summary

This paper presents $CO_2$ Sorting, a new algorithm to retrieve cloud-top altitude using high spectral resolution infrared measurements. The $CO_2$ Sorting algorithm is combined with the established $CO_2$ Slicing algorithm to improve estimates of cloud-top altitude. This new retrieval is applied to observation from the S-HIS during the THORPEX campaigns. The analysis includes a comparison of the hyperspectral algorithms with the active Cloud Physics Lidar system (CPL) measurements capable of independently retrieving the absolute cloud-top altitude as well as cloud optical depth. Additionally Modis Airborne Simulator (MAS) measurements are collocated with the S-HIS fovs to determine the fractional cloud coverage in the S-HIS fov. From these comparisons the sensitivity of these passive IR algorithms is investigated, and it is demonstrated that the combined $CO_2$ Slicing/Sorting algorithm performs best for optically thin clouds with significantly reduced cloud height biases compared to the standard fix channel pair $CO_2$.Slicing.

Future research plans include applications to additional aircraft measurements and continued development of the $CO_2$ Slicing/Sorting retrieval to improve the sensitivity of the algorithm to low clouds. Implementation of the $CO_2$ Slicing/Sorting retrieval to satellite based hyperspecteral measurements (AIRS) are planned.

## Acknowledgements

The authors would like to gratefully thank the S-HIS research team for supplying the S-HIS measurements used in this paper. We would like to acknowledge Ray Garcia for his help with understanding the S-HIS data processing. We would like to thank the MAS instrument and cloud mask research groups for supplying the MAS measurements and

cloud mask. The NASA Goddard Suomi-Simpson fellowship program funded this research.

## References

Ackerman, S. A., K. I. Stabala, W. P. Menzel, R. A. Frey, C. Moeller, and L. E. Gumley, 1998: Discriminating clear sky from clouds with MODIS. *Journal of Geophysical Research*, **103,** 32141-32157.

Bayler, G. M., R. M. Aune, and W. H. Raymond, 2000: NWP cloud intialization using GOES sounder data and improved modeling of nonprecipitating clouds. *Monthly Weather Review*, **128,** 3911-3920.

Chahine, M. T., 1974: Remote sounding of cloudy atmospheres. I; The single cloud layer. *Journal of Atmospheric Sciences*, **31,** 233-243.

Clough, S. A., F. X. Kneizys, L. S. Rothman, and W. O. Gallery, 1981: Atmospheric Spectral Transmittance and Radiance - Fascod1b. *Proceedings of the Society of Photo-Optical Instrumentation Engineers*, **277,** 152-166.

Huang, H. L., W. L. Smith, L. Li, P. Antonelli, X. Wu, R. O. Knuteson, B. Huang, and B. J. Osborne, 2003: Minimum local emissivity variance retrieval of cloud altitude and effective spectral emissivity simulation and initial verification. *Journal of Applied Meteorology*, **43,** 795-809.

Kim, D. B., S.G. and J. M. Brown, 2002: Cloud/hydrometeor initialization in the 20-km RUC using radar and GOES data. *15th Conference on Numerical Weather Predictoin*, San Antonio, TX, 355-338.

King, M. D., W. P. Menzel, P. S. Grant, J. S. Myers, T. G. Arnold, S. E. Platnick, L. E. Gumley, S. Tsay, C. C. Moeller, M. Fitzgerald, K. S. Brown, and F. G. Osterwisch, 1996: Airborn Scanning Spectrometer for Remote Sensing of Cloud, Aerosol, Water Vapor, and Surface Properties. *Jounal of Atmopheric and Oceanic Technology*, **13,** 777-794.

McGill, M., D. Hlavka, W. Hart, V. S. Scott, J. D. Spinhirne, and B. Schmid, 2002: Cloud Physics Lidar: instrument description and initial measurement results. *Applied Optics*, **41,** 3725-3734.

McGill, M. J., 2004: CPL Cloud Optical Depth Sensitivity.

McNally, A. P. and P. D. Watts, 2003: A cloud detection algorithm for high-spectral-resolution infrared sounders. *Quarterly Journal of the Royal Meteorological Society*, **129,** 3411-3423.

Menzel, W. P. and J. F. W. Purdom, 1994: Indroducing GOES-I: the first of a new generation of geostationary operational environmental satellites. *Bulletin of the American Meteorological Society*, **75,** 757-781.

Menzel, W. P., L. W. Smith, and T. R. Stewart, 1983a: Improved cloud motion wind vector and altitude assignment using VAS. *Journal of Applied Meteorology*, **22,** 377-384.

Menzel, W. P., W. L. Smith, and T. R. Stewart, 1983b: Improved Cloud Motion Wind Vector and Altitude Assignment Using Vas. *Journal of Climate and Applied Meteorology*, **22,** 377-384.

Nagel, F. W., 1998: The Association of Disparate Satellite Observations. *Second Symposium of Integrated Observing Systems*, Phoenix AZ, The American Meteorological Society.

Ohring, G., B. Wielicki, R. Spencer, B. Emery, and R. Datla, 2002: Satellite instrument calibration for measuring global climate change, 101 pp.
Revercomb, H. E., V. P. Walden, J. Tobin, F. A. Anderson, N. C. Best, N. C. Ciganovich, T. G. Dedecker, T. Dirkx, S. C. Ellington, R. K. Garcia, R. Herbsleb, R. O. Knuteson, D. LaPorte, D. McRae, and M. Werner, 1998: Recent Results From Two New Aircraft-Based Fourier-Transform INterferometers: The Scannign High-resolution Interferometer Sounder adn the NPOESS Atmospheric Sounder Testbed Interferomter. *8th International Workshop on atmospheric Science from Space Using Foourier Transform Spectrometry*, Toulouse, France.
Schrieniner, A. J., T. J. Schmit, and M. W.P, 2001: Observations and trends of clouds based on GOES sounder data. *Journal of Geophysical Research-Atmospheres*, **106,** 20,349-20,363.
Schutz, B. E., 1998: Spaceborne laser altimetry: 2001 and beyond, 4 pp.
Shapiro, M. A. and A. J. Thorpe, 2002: The observing-system research and predictability experiment, 16 pp.
Smith, W. L., 1970: A regression method for obtaining real-time temperature and geopotential height profiles from satellite spectrometer measurements and its aplication to Nimbu-3 SIRS observations. *Monthy Weather Review*, **98,** 604-611.
Smith, W. L. and C. M. R. Platt, 1978: Comparison of Satellite-Deduced Cloud Heights with Indications from Radiosonde and Ground-Based Laser Measurements. *Journal of Applied Meteorology*, **17,** 1796-1802.
Smith, W. L. and R. Frey, 1990: On Cloud Altitude Determinations from High-Resolution Interferometer Sounder (His) Observations. *Journal of Applied Meteorology*, **29,** 658-662.
Smith, W. L., H. M. Wolf, P. G. Abel, C. M. Hayden, M. Chalfant, and N. Grody, 1974: Nimbus 5 sounder data processing system, 1, Measurement characteristics and data reduction procedures, 99 pp.
Smith, W. L. P., M.R., 1978: Intercomparison of radiosonde, ground based laser, and satellite deduced cloud heights. *Journal of Applied Meteorology*, **17,** 1796-1802.
Winker, D. M. and B. Wielicki, 1999: PICASSO-CENA mission. *Sensors, systems, and next-generation satellites III*, SPIE, 26-36.
Wylie, D. P., 1994: Four Years of Global Cirrus Cloud Statistics Using HIRS. *Journal of Climate*, **7,** 1972-1986.
Wylie, D. P. and W. P. Menzel, 1989: Two years of cloud cover statistics using VAS. *Journal of Climate*, **2,** 380-392.

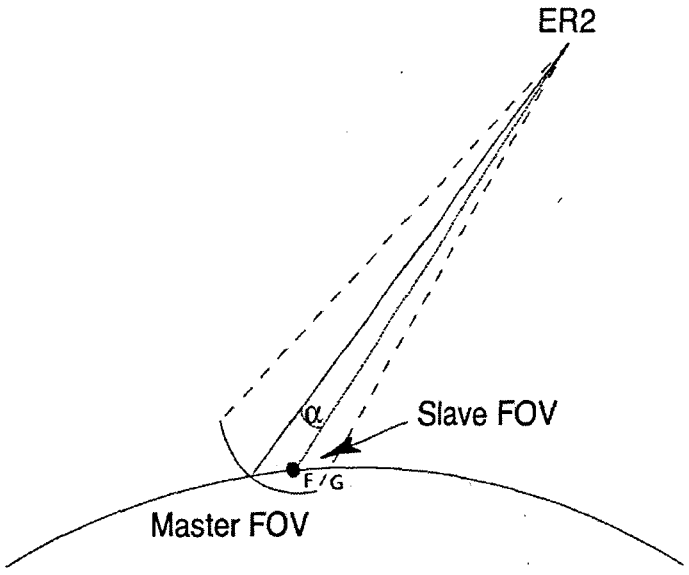


**Figure 1** The collocation algorithm geometry is illustrated. The master field of view is defined as the half angular field of view of the master instrument (S-HIS). The angle between the slave instrument (MAS or S-HIS) geo-location (F) and the center axis of the master field is designated α in this figure. If α is less than the half angular field of view of the master instrument the slave pixel is considered to be within the field of view of the S-HIS.

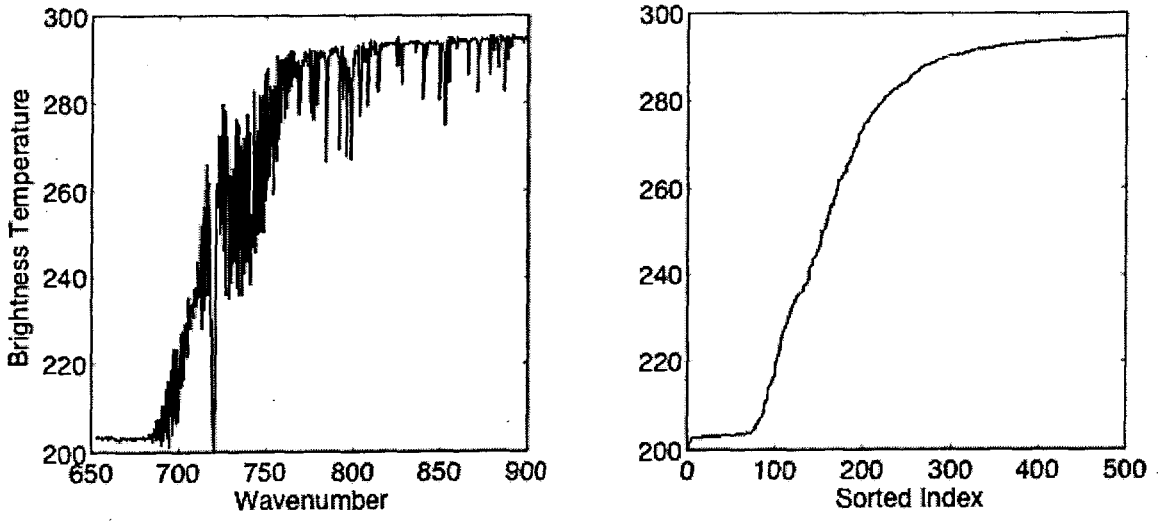


**Figure 2** The S-HIS brightness temperature spectrum for the $CO_2$ absorption band is presented on the right figure. The right figure presents the brightness temperatures sorted from the coldest to warmest channels.

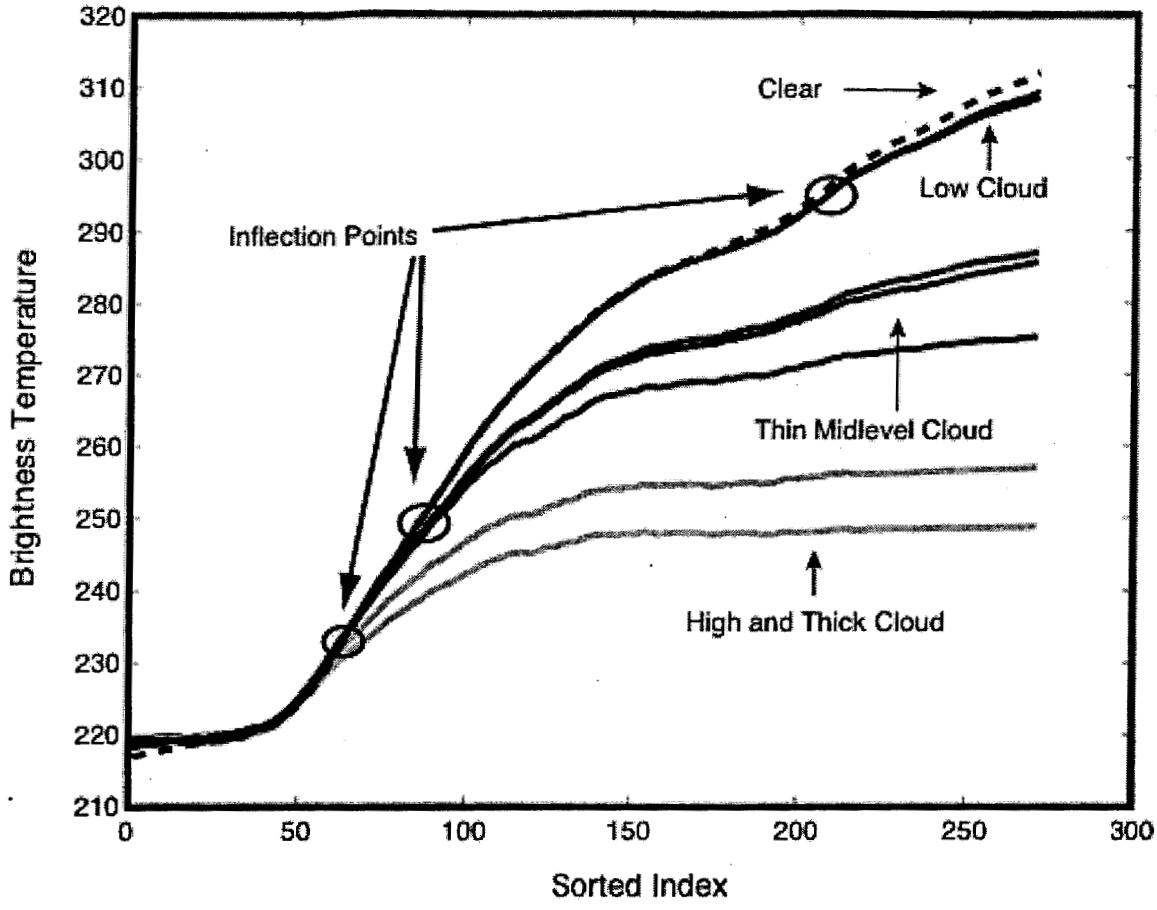


**Figure 3** The clear sky sorted index applied to low, high, and optically thin S-HIS cloudy field of view (FOV). The dashed curve is the sorted clear sky FOV. The inflection points are circled in the figure.

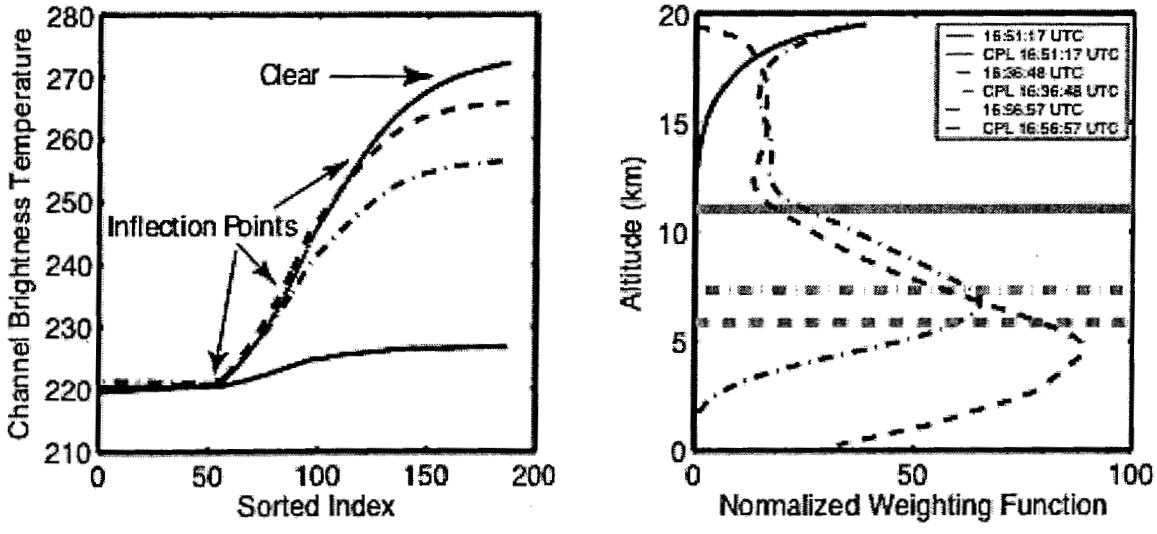


**Figure 4** Cloudy sorted BT spectrums are presented with the clear sky sorted BT. The weighting functions of the channel picked to be the inflection point in the right figure are

presented on the left. The horizontal lines cloud height determined using the collocated CPL measurement is included in the figure to the right.

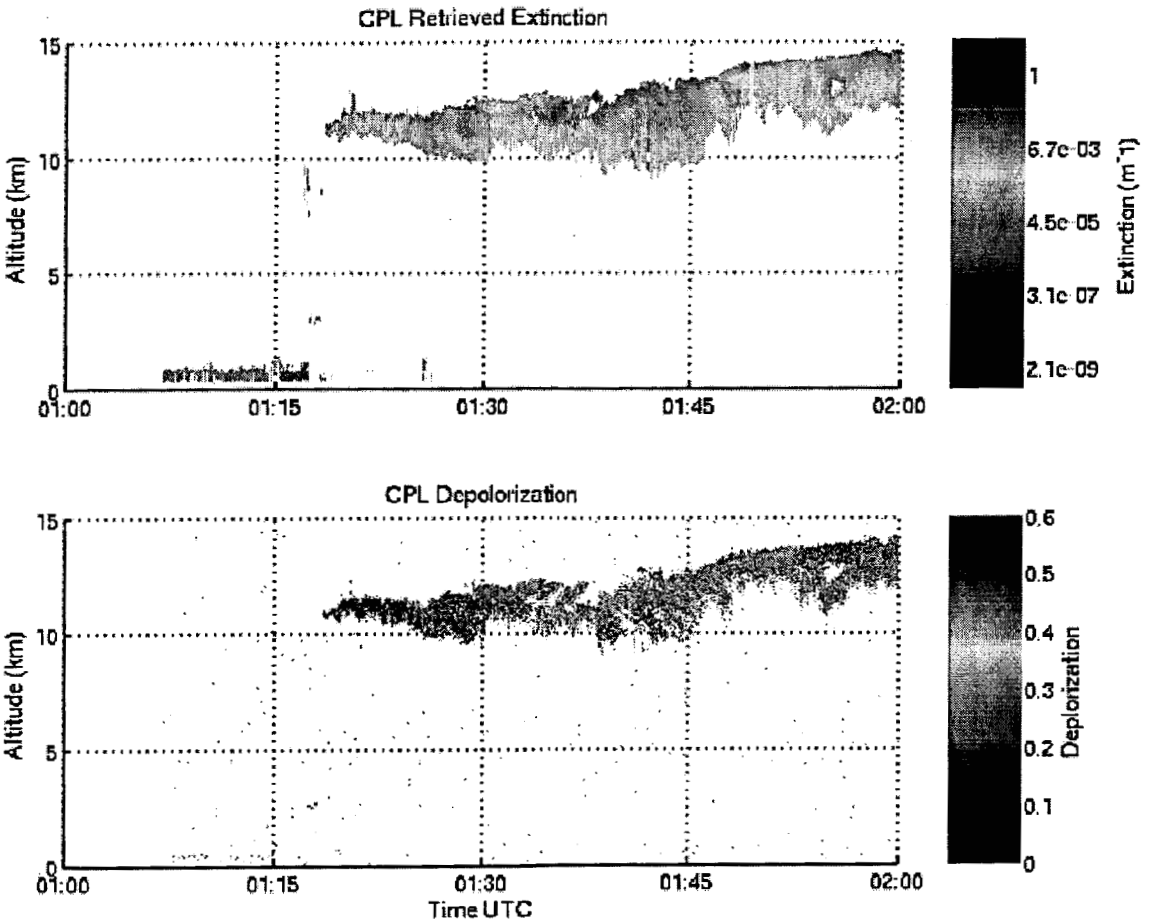


**Figure 5** The CPL retrieved extinction and depolarization cross-sections for the February 22nd THORPeX flight.

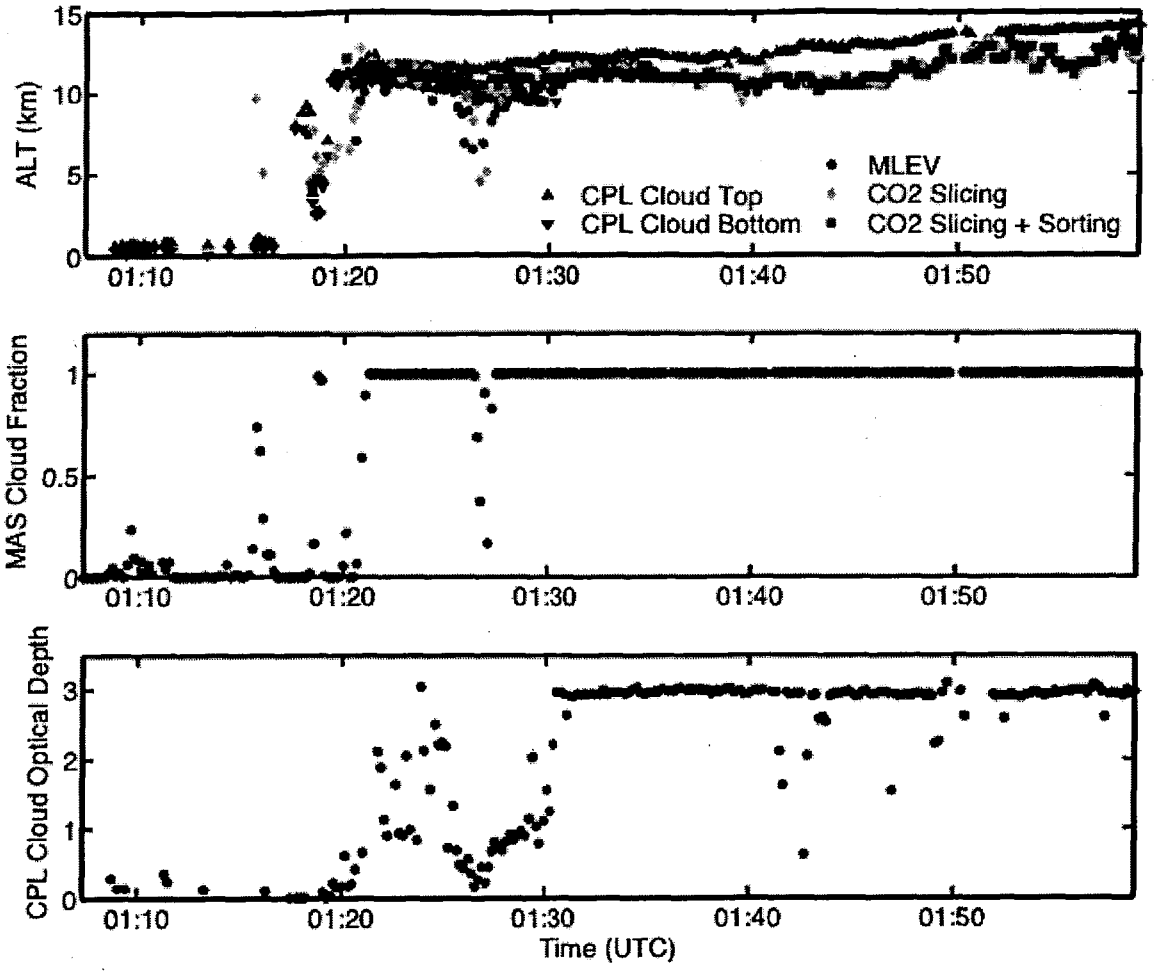


**Figure 6** The S-HIS cloud-top retrievals collocated with the CPL measured cloud-top and base measurements from February 22nd 2003 (top panel). The SHIS cloud fraction is computed using the collocated MAS cloud mask (middle panel). The mean CPL measured optical depth is presented in the bottom figure. The cloud-top, base and optical depth are the mean of all the CPL measurements found to be in each S-HIS field of view.

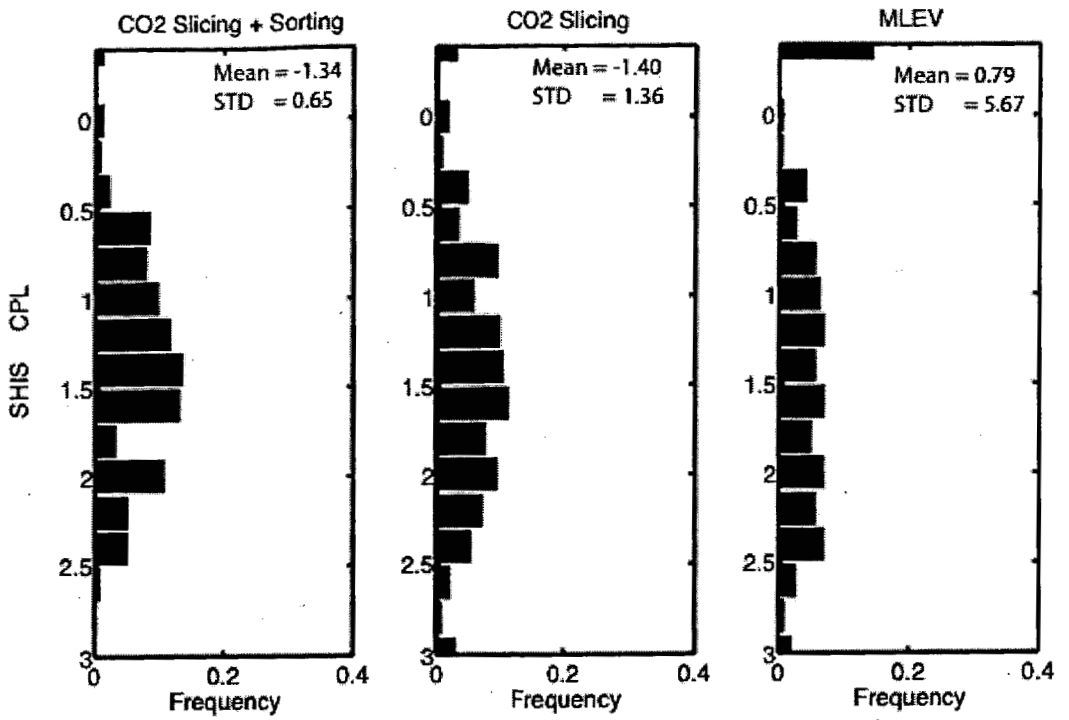


**Figure 7** The frequency of occurrence of the differences between the S-HIS cloud-top retrieval height compared to the mean of the collocated CPL cloud height for the different S-HIS retrievals for the February 22nd 2003 flight.

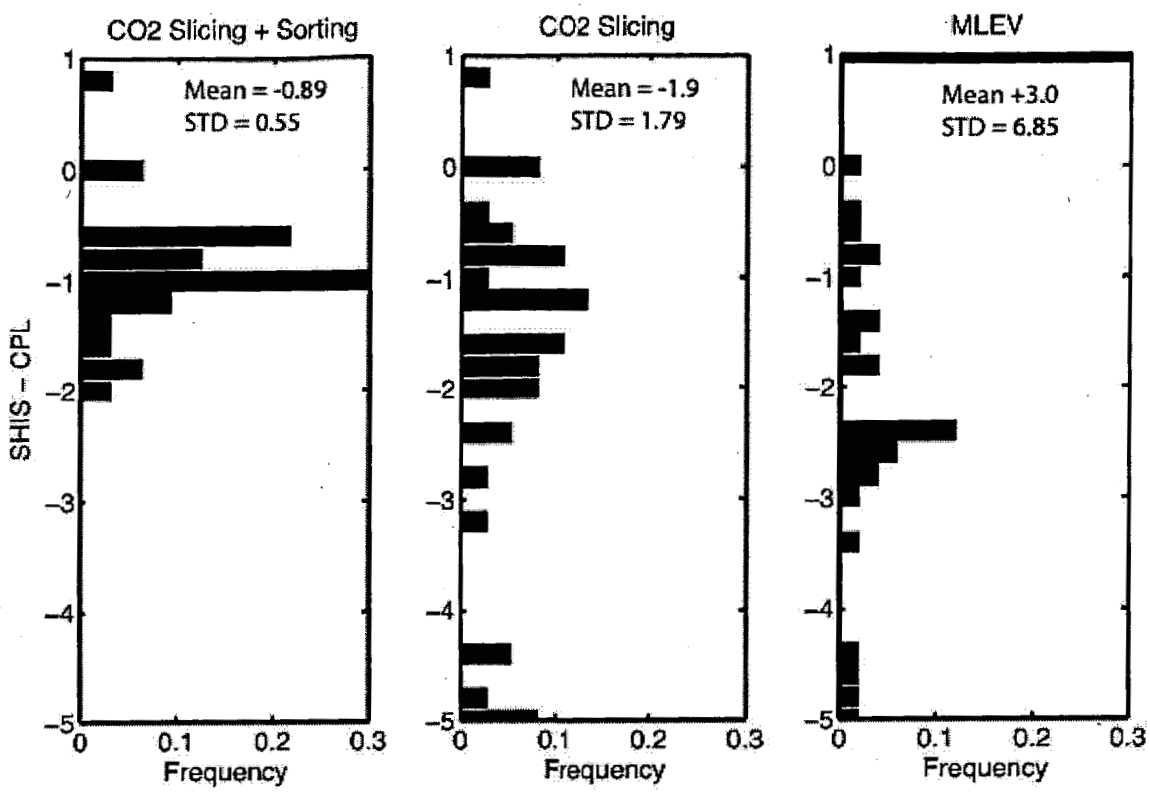


**Figure 8** The frequency of occurrence of the differences between the S-HIS cloud-top retrieval height compared to the mean of the collocated CPL cloud height for S-HIS fov with CPL measured cloud optical thickness less then 1.0 for the S-HIS retrievals for the February 22nd 2003 flight.

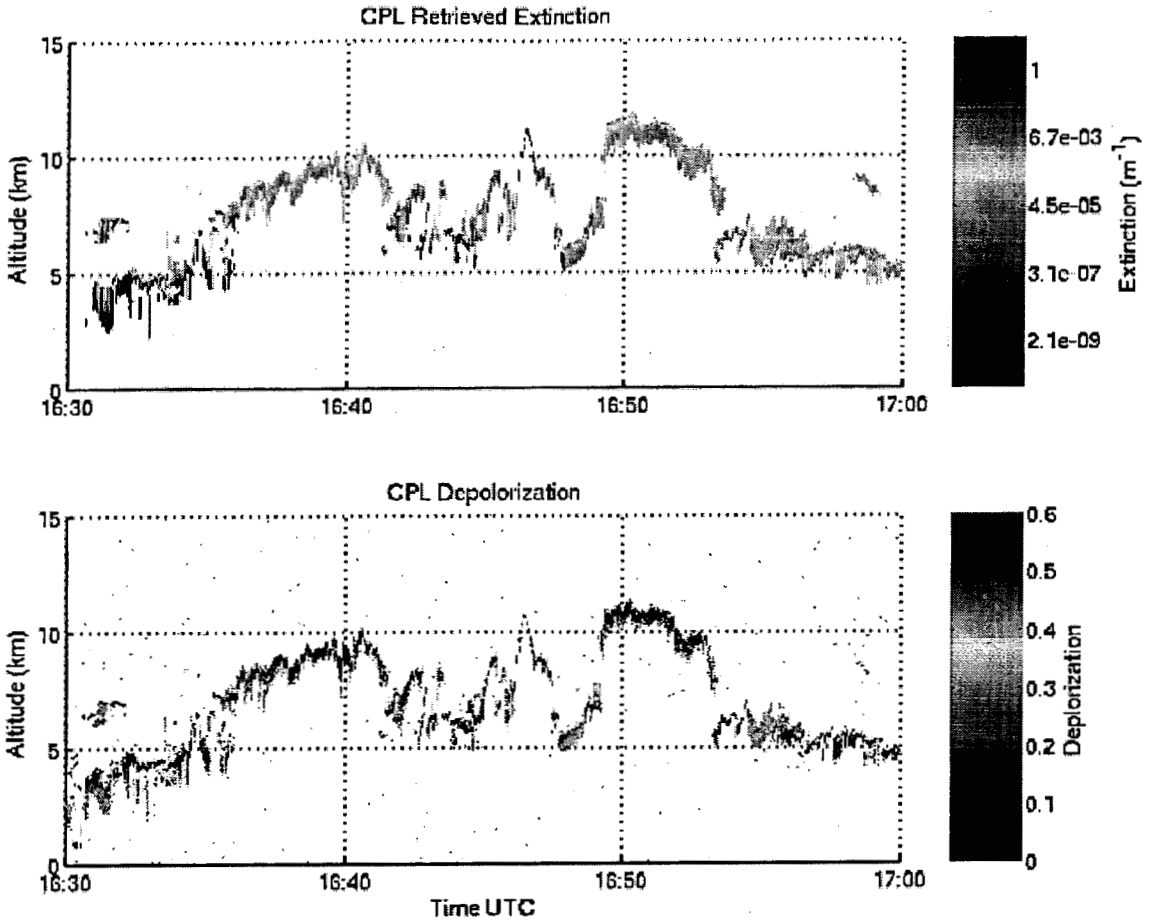


**Figure 9** The CPL retrieved extinction and depolarization from the Atlantic THORPeX experiment on December 5th 2003.

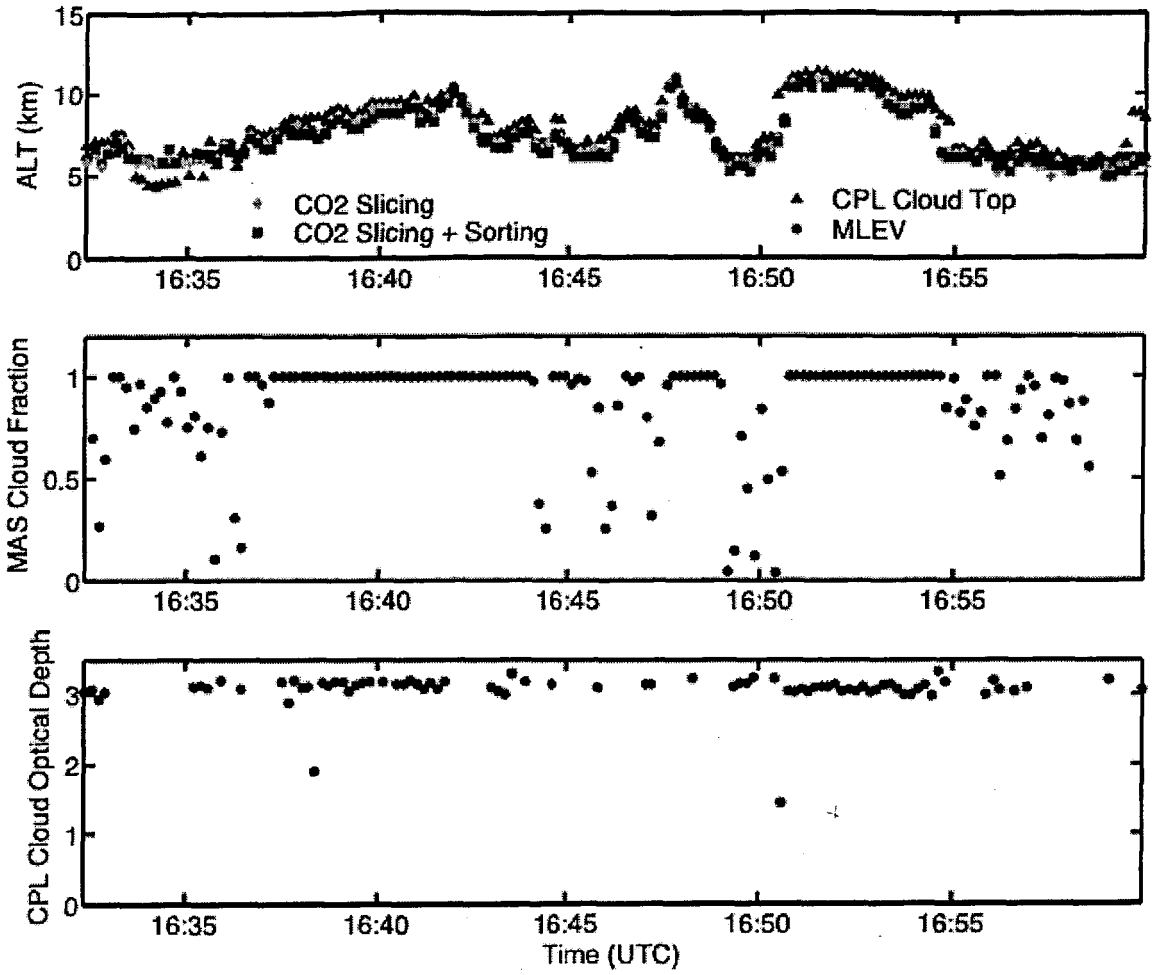


**Figure 10** The S-HIS cloud-top retrievals collocated with the CPL measured cloud-top and base measurements from December 5th 2003 (top panel). The cloud fraction is computed using the collocated MAS pixels for each S-HIS field of view (middle panel). The MAS cloud mask is applied to the collocated MAS pixels and the cloud fraction is computed from the cloud mask results. The mean CPL measured optical depth is presented in the bottom panel. The cloud-top, base and optical depth are the mean of all the CPL measurements found to be in each S-HIS field of view.

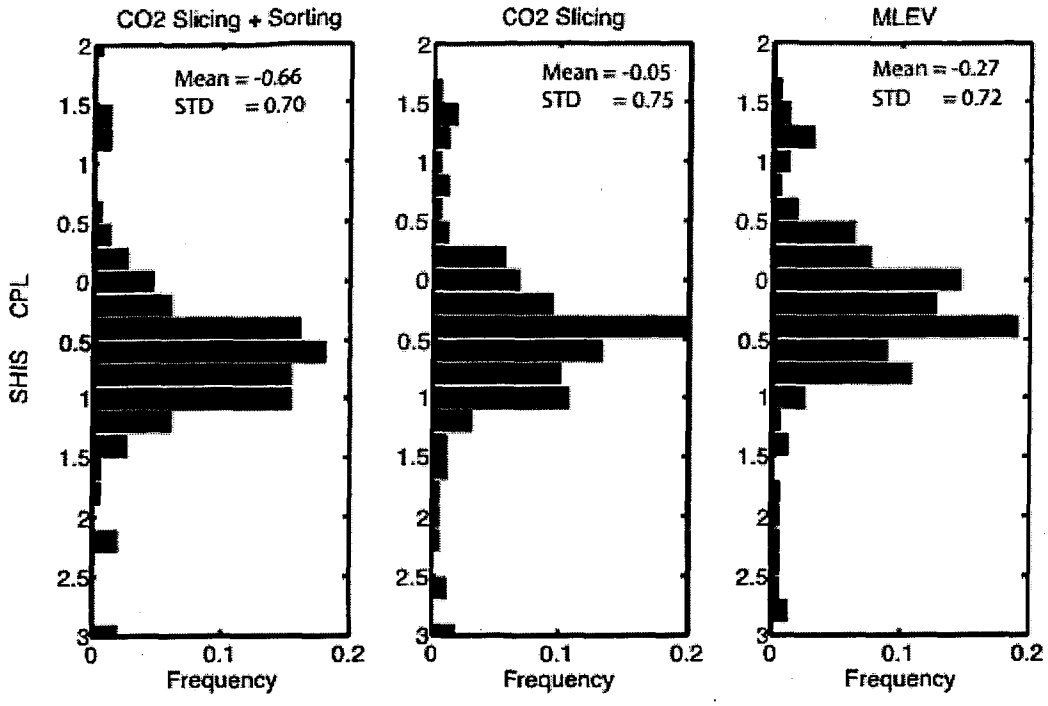


**Figure 11** The frequency of occurrence of the differences between the S-HIS cloud-top retrieval height compared to the mean of the collocated CPL cloud height is presented for the different S-HIS retrievals for the flight on December 5th 2003.

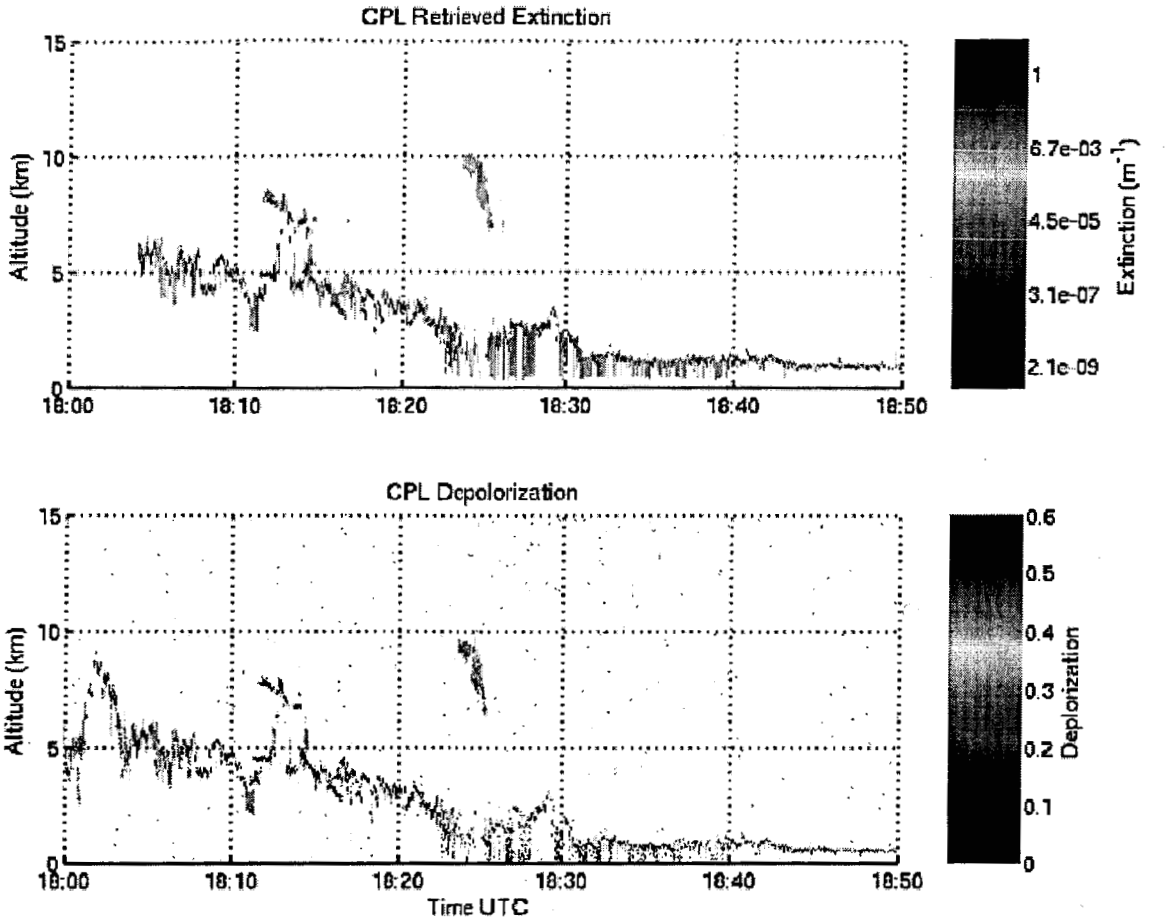


**Figure 12** The CPL retrieved extinction and depolarization from the Atlantic THORPeX experiment on December 5th 2003.

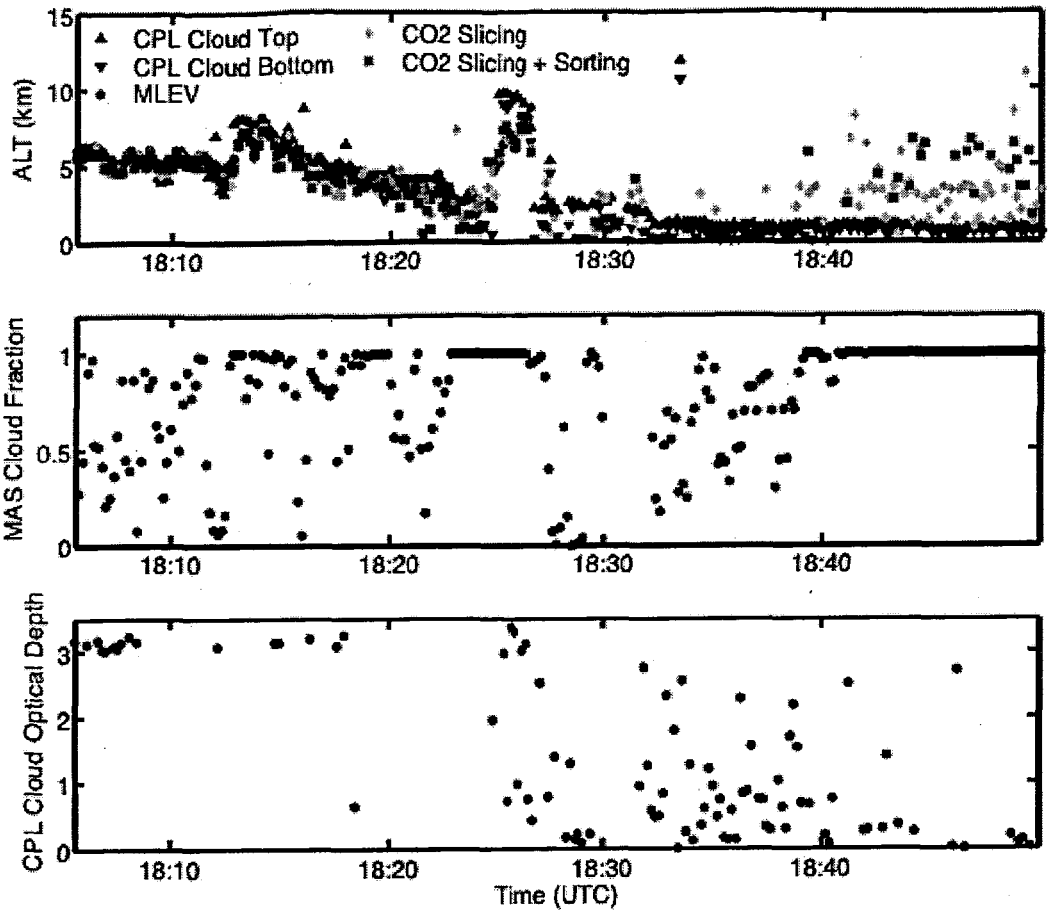


**Figure 13** The S-HIS cloud-top retrievals collocated with the CPL measured cloud-top and base measurements from December 5th 2003 (top panel). The MAS cloud fraction is presented in the middle panel and the mean CPL measured optical depth in the bottom figures. The cloud-top, base and optical depth are the mean of all the CPL measurements found to be in each S-HIS field of view.

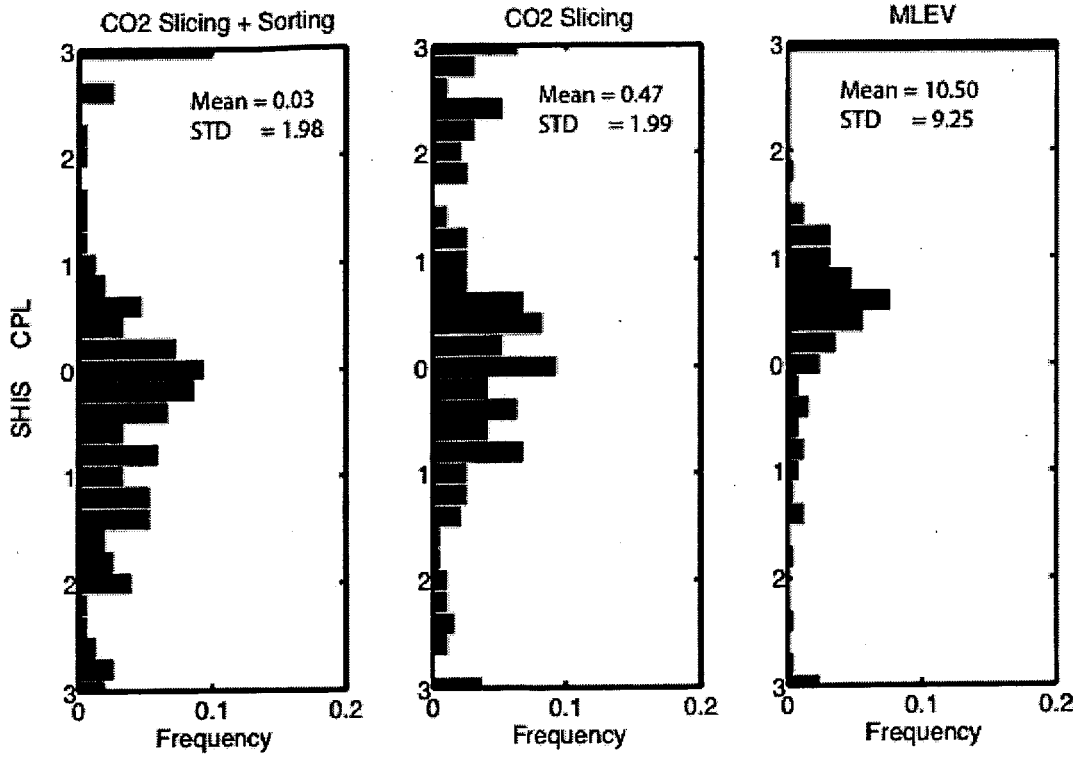


**Figure 14** The frequency of occurrence of the differences between the S-HIS cloud-top retrieval height compared to the mean of the collocated CPL cloud height is presented for the different S-HIS retrievals for the flight on December 5th 2003

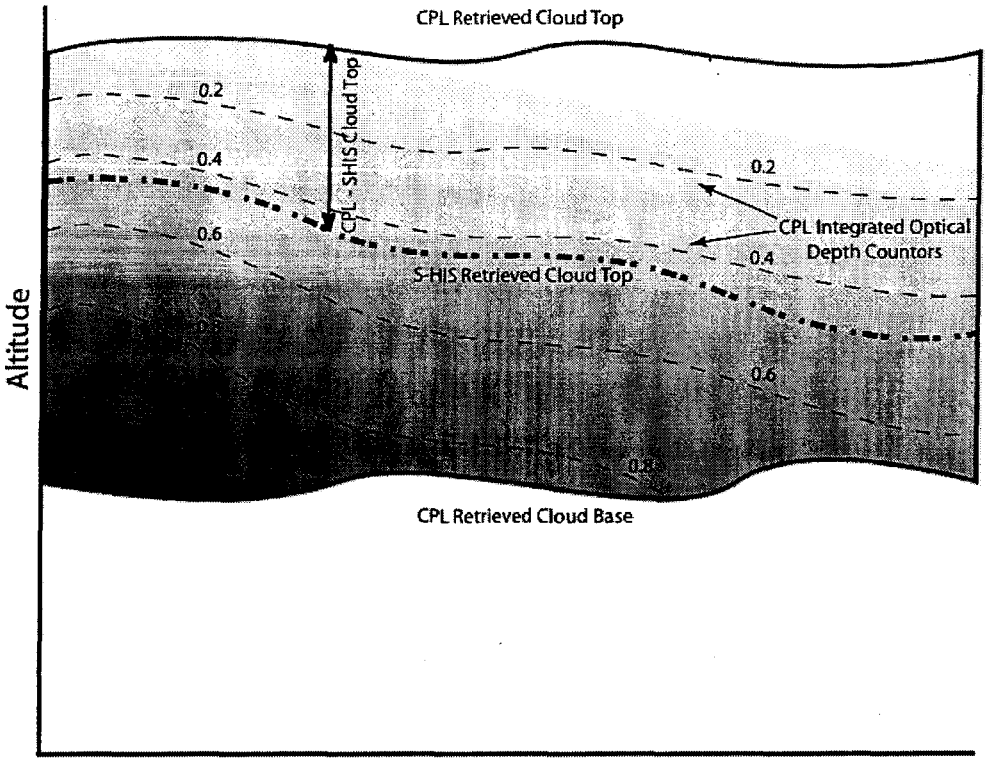


**Figure 15** The method to determine the CPL integrated cloud optical depth at the level of the SHIS retrieval. The optical depth contours are determined by integrating the CPL extinction profile through the cloud.

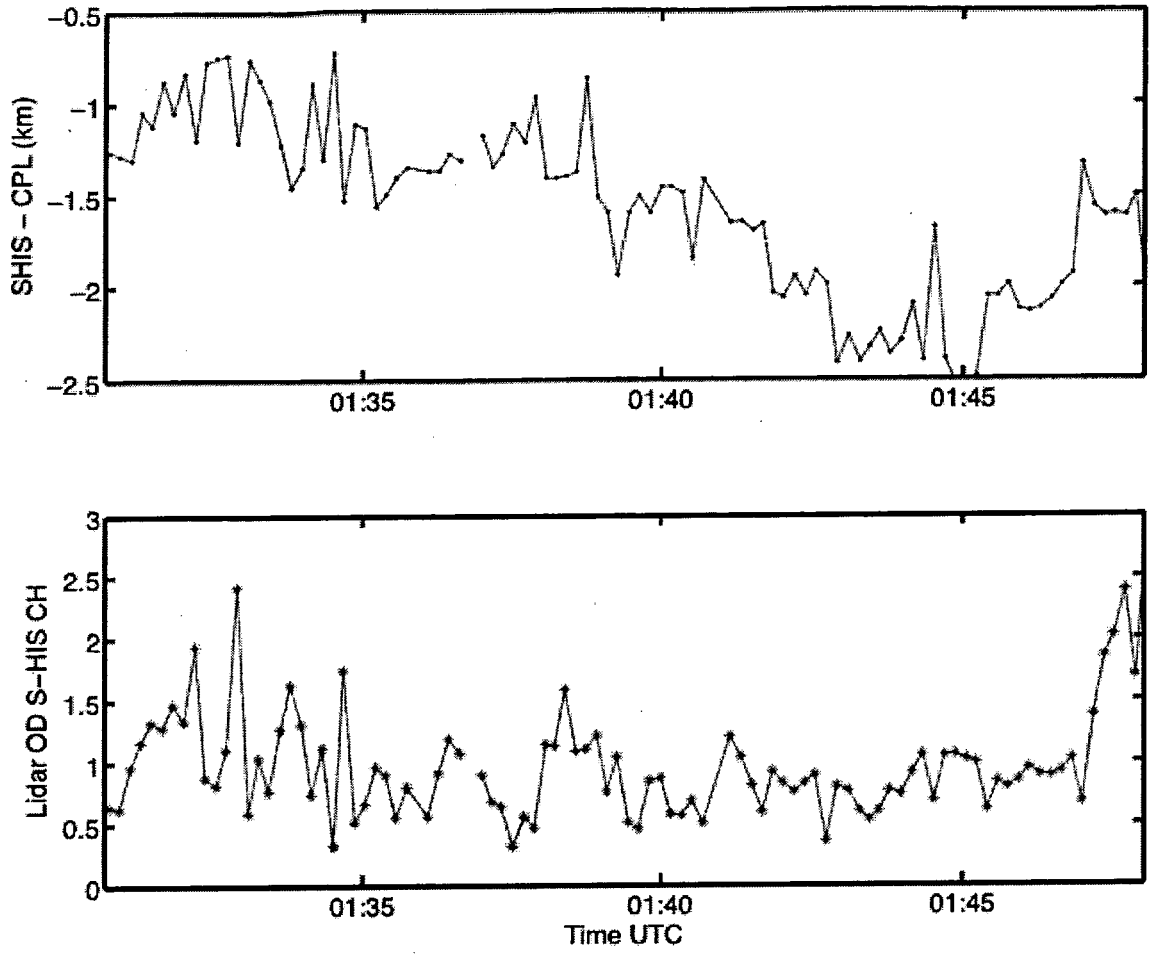


**Figure 16** The geometric difference between the SHIS hybrid slicing/sorting retrieval and the collocated CPL cloud height for the February 22 flight is presented in this figure. The integrated optical depth determined by the CPL at the level of the S-HIS hybrid retrieved cloud height is presented in the lower plot. Notice that integrated optical depth remains relatively constant while the SHIS – CPL cloud height differences vary between 0.5 – 5.0 km.

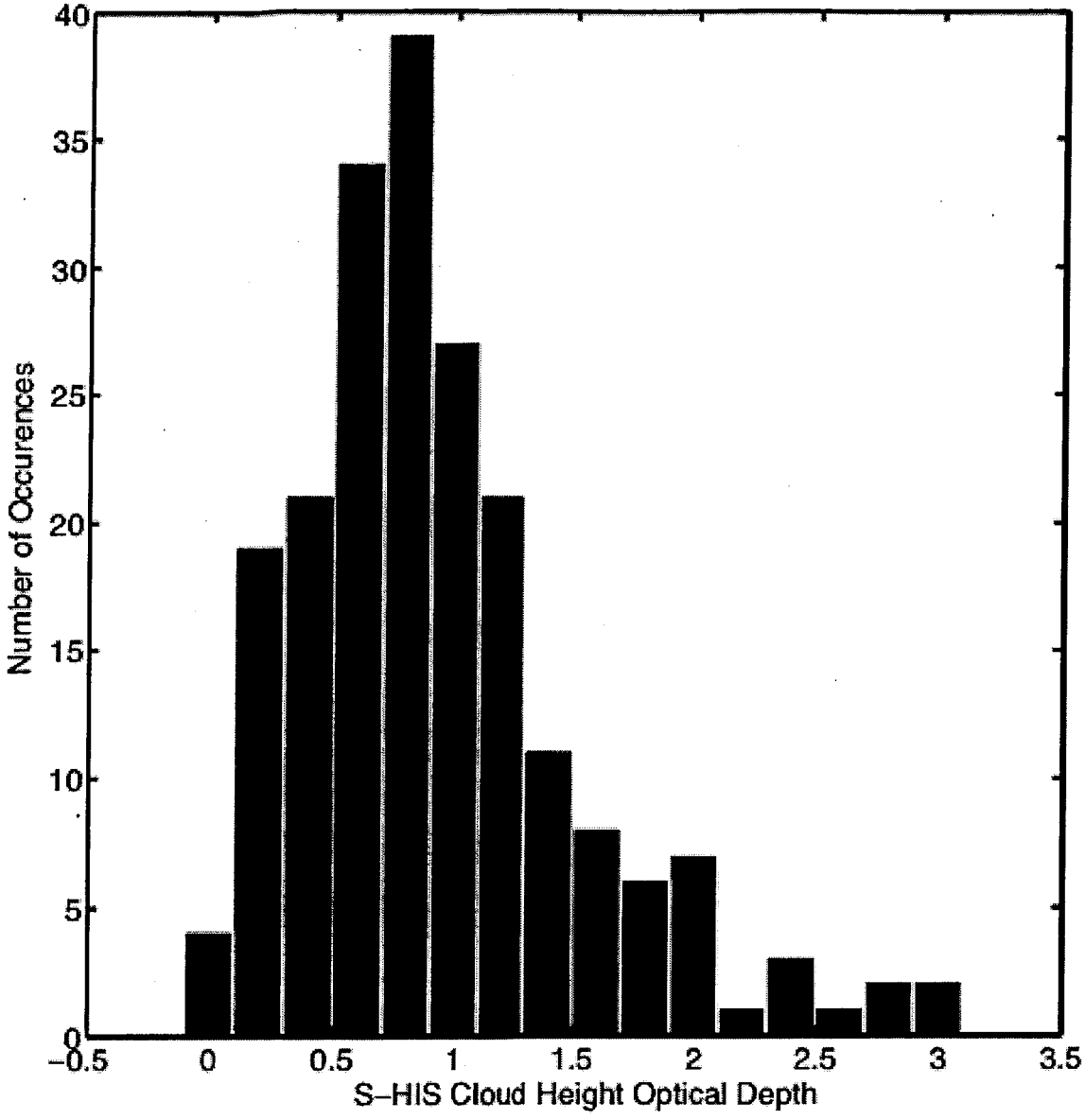


**Figure 17** The frequency of occurrence of the CPL integrated optical depth at the level of the S-HIS $CO_2$ Sorting/Slicing hybrid retrieved cloud height from the February 22 ER2 flight between 1:07 – 2:00 UTC is presented in this figure. Notice the optical depths peak between 0 – 1.0.